Microfabricated Arrays of Cylindrical Wells Facilitate Single-Molecule Enzymology of α-Chymotrypsin

Angela Y. Chen and Ashish S. Jani
Dept. of Biomedical Engineering, Henry Samueli School of Engineering, University of California, Irvine, CA 92697

Lifeng Zheng
Dept. of Electrical Engineering and Computer Science, Henry Samueli School of Engineering, University of California, Irvine, CA 92697

Peter J. Burke
Dept. of Biomedical Engineering, Henry Samueli School of Engineering, University of California, Irvine, CA 92697

Dept. of Electrical Engineering and Computer Science, Henry Samueli School of Engineering, University of California, Irvine, CA 92697

James P. Brody
Dept. of Biomedical Engineering, Henry Samueli School of Engineering, University of California, Irvine, CA 92697

DOI 10.1021/bp.283
Published online July 16, 2009 in Wiley InterScience (www.interscience.wiley.com).

Single-molecule enzymology allows scientists to examine the distributions of kinetic rates among members of a population. We describe a simple method for the analysis of single-molecule enzymatic kinetics and provide comparisons to ensemble-averaged kinetics. To isolate our model enzyme, α-chymotrypsin, into single molecules, we use an array of cylindrical poly(dimethylsiloxane) wells 2 μm in diameter and 1.35 μm in height. Inside the wells, a protease assay with a profluorescent substrate detects α-chymotrypsin activity. We hold the concentration of α-chymotrypsin at 0.39 nM in a given well with an enzyme-to-substrate ratio of 1:6,666 molecules. Fluorescence emitted by the substrate is proportional to enzyme activity and detectable by a charge-coupled device. This method allows for the simultaneous real-time characterization of hundreds of individual enzymes. We analyze single-molecule kinetics by recording and observing their intensity trajectories over time. By testing our method with our current instruments, we confirm that our methodology is useful for the analysis of single enzymes for extracting static inhomogeneity. © 2009 American Institute of Chemical Engineers *Biotechnol. Prog.,* 25: 929–937, 2009
Keywords: single-molecule enzymology, microfabricated array, chymotrypsin

Introduction

Enzymology at the single-molecule level offers a more accurate characterization of enzyme dynamics than ensemble kinetics in several ways. When studied as an ensemble, enzyme activity is averaged and requires synchronization of each molecule for the purpose of representing the population's kinetic trend as one.[1–3] The ensemble average overlooks detailed enzymatic distributions among members of the population, where each individual enzyme could be present at a different stage along a reaction sequence at the time of measurement.[1] By conducting single-molecule studies of an enzyme, the kinetics of individual enzyme molecules can be traced more directly than ensemble-averaged studies.[4] The direct measurement of single-molecule trajectories provides specific statistical information on individual enzyme distributions, whereas ensemble kinetics is limited to rendering the mean value.[5] Furthermore, ensemble kinetics is unable to detect either static or dynamic inhomogeneity.[6] Static inhomogeneity refers to how single-enzyme molecules exhibit distinct and stable rate constants over long periods while dynamic inhomogeneity describes the temporal fluctuations of kinetic rates in individual molecules.[6,7] It is important to note that occurrences of static and dynamic inhomogeneities are not exclusive. The temporal fluctuations of kinetic rates occur because of conformational changes of enzymes.[8] The same enzyme existing in various substates at different points in time may possess different catalytic efficiencies.[4] Single-molecule studies using small containers not only allow desirable localizations of the enzyme and the depiction of unusual or transient species that are averaged in ensemble studies but also the ability to delineate static and dynamic inhomogeneities.[3] In many enzymes, conformational dynamics have also been observed in bound and unbound positions.[9] Hence, conducting single-molecule enzymology is extremely important in extracting detailed enzymatic kinetics, and we will use α-chymotrypsin as our

Correspondence concerning this article should be addressed to J. P. Brody at jpbrody@uci.edu.

model enzyme to test the proposed methodology for static inhomogeneity.

The serine protease, α-chymotrypsin, has been examined thoroughly in ensemble studies but not quite extensively as a single molecule. A few publications have examined α-chymotrypsin at the single-molecule level, such as the water-in-oil emulsion method previously described by our lab.[10] Also, a simulation tool called Targeted Molecular Dynamics (TMD) has been used recently to study the stepwise activation of wild type and mutant Δα-chymotrypsin at the single-molecule level, allowing correlation to ensemble experiments.[11] Furthermore, the deactivation of α-chymotrypsin was also revealed as a stepwise process by entrapping individual molecules of the enzyme in agarose polymers.[12] Unraveling the kinetics of α-chymotrypsin as a single molecule will fortify our knowledge of this enzyme's metabolic and proteolytic function.[12]

Chymotrypsinogen is first produced by the pancreas as a zymogen, which is cleaved by trypsin to become chymotrypsin in the small intestine.[13,14] The protease α-chymotrypsin is a 25 kDa protein with 241 amino acid residues.[15] The cleavage site targeted by α-chymotrypsin is the peptide bond following large hydrophobic amino acid residues, such as tyrosine, tryptophan, and phenylalanine in potential substrates.[16,17] Although the main function of α-chymotrypsin is to digest dietary protein, it also plays an important role in the immune system.[14,18] A recent study has shown that there are both antimicrobial and immunostimulatory activities in the hydrolysate of protein digestion in food by proteolytic enzymes, such as α-chymotrypsin and trypsin.[18] Hence, it is important to study α-chymotrypsin at the single-molecule level in order to further investigate its biochemical properties. We examine α-chymotrypsin's single-molecule kinetics by using a method that combines protease assays, nanotechnology, and fluorescence microscopy. First, let us evaluate our prior method of single-molecule enzymology for α-chymotrypsin.

Previously, we used a water-in-oil emulsion method to isolate α-chymotrypsin into single molecules. An oil phase consisting of silicon oil was mixed together with a water phase, containing the enzyme and the substrate. This process generates water-in-oil droplets that act as vessels for single-molecule isolation of α-chymotrypsin.[10] Two major problems with the water-in-oil emulsion method included difficulty in creating uniformly sized droplets to enclose individual enzymes and difficulty in capturing all droplets in a single plane by a charge-coupled device (CCD).

We attempt to improve the water-in-oil emulsion method by using an array of microfabricated wells that are fixed in volume.[19,20] The array of cylindrical wells allows for the simultaneous observation of hundreds of individual enzymes over time, and the diameter and height of the wells can be easily controlled by design. Given α-chymotrypsin's diameter at 4.4 nm estimated by X-ray crystallography and our single well dimensions, 2 μm in diameter and 1.35 μm in height, our wells will be able to enclose the individual enzymes.[21]

Methods based on small reaction containers have been published for the analysis of various enzymes. Arrays of femtoliters chambers were initially established by Hiroyuki Noji's group at the University of Tokyo to study horseradish peroxidase and β-galactosidase.[19] Currently, an application of this method for single-molecule enzymology is seen in the fast-mixing microfluidics device that utilizes an array of cylindrical chambers designed 5 μm in diameter to control and evaluate reaction initiation of β-galactosidase.[20] In the past, femtoliter vials have been used to study single molecules of lactate dehydrogenase (LDH-1), and more than 100 molecules of the enzyme can be observed simultaneously.[22] The heterogeneity of LDH-1's activity was observed in comparison with single metal ions that showed unvarying catalytic activity.[22] A recent method of single-molecule enzymology has been presented in literature by David R. Walt's group at the Tufts University.[7] This method utilizes optical fiber bundles that contain femtoliter arrays with wells 2.5-μm deep and a volume of 40 fL to study hundreds of individual β-galactosidase molecules.[7] In addition, colloidal crystals with diameters on the order of nanometers have lately been described as a novel single-molecule matrix for the analysis of horseradish peroxidase.[23] By adjusting the pH, the capsid of a virus can disintegrate and reassemble for single-molecule studies of horseradish peroxidase.[24] In this article, we examine the kinetics of α-chymotrypsin by performing a single-protease assay inside an array of cylindrical wells each with a volume of 4.24 fL.

Materials and Methods

Instruments

We conducted ensemble experiments in the ThermoLabsystems Fluoroskan Ascent® FL fluorescence microplate reader using a filter set with excitation wavelength of 565/25 nm and emission wavelength of 630/30 nm. A quartz-halogen lamp served as the light source, and a photomultiplier tube detected fluorescence signals.

Our single-molecule experiments were performed in an epi-fluorescence Nikon ECLIPSE TE200 inverted microscope. The light source for our microscope was a 100 watt Nikon mercury lamp. We purchased a filter cube (Chroma #41027) with excitation and emission wavelengths of 580/20 and 630/60 nm, respectively. For filter selection, we used the filter set that allowed maximal photon capture among four filter set candidates. The amount of energy the specimen absorbed and the final signal the specific filter set produced were our selection criteria. A Nikon Plan Fluor 40× oil-immersion objective (Numerical Aperture 1.3) was used to observe the specimen. An Apogee Ap7p, 16-bit, back-illuminated CCD was employed as the fluorescence detection unit. Our CCD camera has a chip with a photon-sensitive 512 × 512 pixel array. At 630 nm, the CCD camera has a quantum efficiency (QE) of 85%.

Protease assays

We purchased bovine α-chymotrypsin from Sigma (#C-7762), which served as the enzyme in our experiments. The EnzChek Protease Assay Kit for red fluorescence from Invitrogen (Molecular Probes #E-6639) provided the substrate. The substrate, which is lyophilized from phosphate-buffered saline, consists of a casein molecule conjugated to five to six molecules of boron dipyrromethene (BODIPY) Texas Red dyes on average.[25] The BODIPY chromophore is structurally stable and has low sensitivity to solvent polarity and pH.[26] A dye-dye quenching phenomenon renders quenching of the fluorescence from the BODIPY Texas Red dyes before enzyme cleavage for up to 98–99%.[27] During protease

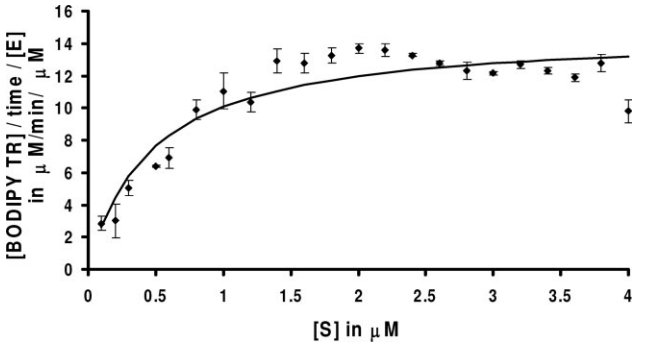

Figure 1. Michaelis-Menten kinetics: Reaction velocity is plotted against substrate concentration.

Enzyme concentration was held at 0.39 nM to ensure that [S] >> [E]. V_m=14.75 min^{-1} and K_m = 0.47 μM. Error bars represent one standard error of mean above and below the mean reaction velocity of three experimental trials we performed. The solid black curve represents the best-fit to the data points shown in this figure using the Lineweaver-Burk equation.

digestion, the dyes produce a 50- to 100-fold increase in fluorescence signal, enhancing fluorescence detection.[27]

Ensemble experiments

In the bulk experiments, we traced the activity of α-chymotrypsin at room temperature over time. By using Invitrogen's EnzChek Protease Assay Kit for red fluorescence (#E-6639) and the Fluoroskan Ascent FL fluorescence microplate reader from ThermoLabsystems, we performed experiments with 96-well black polypropylene round-bottomed assay plates (Corning #07-200-762). We used the filter set with excitation and emission centered at 565/25 and 630/30 nm, respectively.

Ensemble Protease Assays Observing Michaelis-Menten Kinetics. We held the final enzyme concentration at 0.39 nM and the final substrate concentrations at various different concentrations for this experiment. A given well contained 100 μL of solution as the total volume. In each sample, 90 μL of substrate in 1× kit digestion buffer (Tris-HCl) was mixed with 10 μL of enzyme at 3.9 nM in 10 mM HEPES buffer. The blank consisted of 90 μL of 1× kit digestion buffer mixed with 10 μL of 10 mM HEPES. The control consisted of 90 μL of substrate in 1× kit digestion buffer mixed with 10 μL of 10 mM HEPES buffer. We measured the intensity of the blanks, controls, and samples every 3 min for a total of 90 min. Relative fluorescence intensity from the control is subtracted from the raw intensity of the samples to account for background signals. We performed the experiment for a total of three times and presented the mean reaction velocity as a function of substrate concentration in Figure 1. We included error bars in Figure 1 that represent one standard error of mean above and below the mean reaction velocity.

Ensemble Protease Assays for Comparison with Single-Molecule Assays. The blank, control, and samples contained 100 μL total volume in each well. The blank contained 90 μL of 1× kit digestion buffer (Tris-HCl) and 10 μL of 10 mM HEPES buffer. The control contained 90 μL of 2.88 μM substrate in 1× kit digestion buffer mixed with 10 μL of the 10 mM HEPES buffer. The sample contained 10 μL of 3.9 nM of enzyme in 10 mM HEPES buffer mixed with 90 μL of 2.88 μM substrate in 1× digestion buffer. The enzyme-to-substrate ratio was 1:6,666, where the final enzyme and substrate concentration were 0.39 nM and 2.6 μM, respectively. The samples were measured every 3 min for a total duration of 90 min. Background signals obtained in the control group were subtracted from the raw sample signals in each measurement to eliminate background noise.

Table 1. Fabrication Steps of Silicon Mold

Step	Method
1	Thermal deposition of S_iO_2 onto silicon wafer
2	Spin coating of electron-beam (E-Beam) resist
3	E-Beam writing of micro-pillar array structures
4	Post-writing wafer development
5	Metal evaporation of titanium and gold
6	Metal liftoff with organic solution
7	Deep reactive ion etching (DRIE)

Fabrication of the microwell array for single-molecule experiments

The fabrication of the micron-sized cylindrical wells began with the creation of a mold, which consisted of an array of cylindrical pillars on a silicon wafer. The general procedure for the fabrication of our mold is outlined in Table 1. Poly(dimethylsiloxane) (PDMS) was used to produce complementary structures to the mold to form the array of cylindrical wells.

Four-inch silicon wafers were ordered from Silicon Quest International, Inc. by the Integrated Nanosystems Research Facility (INRF) at UC Irvine. These silicon wafers had a thickness of 1 μm of silicon dioxide already deposited on the surface of our wafer. In step 1 of Table 1, an additional 0.3 μm of silicon dioxide was thermally deposited onto the silicon wafer by using a high-temperature furnace at 1,050°C. The resultant thickness of silicon dioxide was ~1.3 μm. In step 2, we used an electron-beam resist, polymethyl methacrylate (PMMA), from MicroChem Corp. The final thickness of PMMA was 270 nm. We used a turntable to spin-coat liquid PMMA onto the wafer initially at 500 rpm for 5 s, followed by 4,000 rpm for 40 s. Subsequently, the wafer was prebaked at 170°C for 15 min on the hot plate to solidify the PMMA. In step 3, we employed the design created in the NPGS (Nanometer Pattern Generation System) from JC Nabity Lithography Systems Version 9.0.109 to conduct electron-beam (E-beam) writing. The wafer was exposed to a 30-kV high energy electron beam, destroying the molecular bonds of PMMA. In the design, the cylindrical pillars were 2 μm in diameter and 1.35 μm in height. The step size was 2 μm, and the array mold was composed of 125 pillars by 125 pillars. The area that the entire array occupied was within a 0.5 mm by 0.5 mm square. In step 4, the silicon wafer was submerged for 60 s in a developing solution composed of methyl isobutyl ketone (MIBK) and isopropyl alcohol (IPA), at 1:3 weight ratio, respectively, in order to dissolve and remove the area of the PMMA exposed to the E-beams. In step 5, metal evaporation of titanium onto the wafer serveed as an adhesive for gold. The total thickness of titanium and gold was ~50 nm. The metals were used to provide a protective layer of selective areas of the wafer for the subsequent etching process. In step 6, selective areas on the wafer were targeted for metal liftoff. The organic solution we used to perform metal liftoff contained acetone and dichloromethane at 1:1 weight ratio. In step 7, deep reactive ion etching (DRIE) was performed

in the Surface Technology Systems (STS) Advanced Silicon Etch (ASE) machine to etch SiO_2 and produce the final pillar structures. We performed four cycles of etching (with O_2 and SF_6) and passivation (with C_4F_8). The duration of etching in each cycle was 8 s and that for passivation was 5 s. Finally, the surface of the wafer containing the pillars was coated with tridecafluoro tetrahydrooctyl silane (TTS) by using a vacuum chamber. TTS was used to facilitate the removal of PDMS from the wafer in subsequent steps for the formation of cylindrical wells.

The cylindrical wells were formed by using PDMS to create complementary structures to the mold. We placed the wafer mold in a polystyrene Petri dish (Fisherbrand #08-757-13) with pillars facing upward, and then we placed the PDMS solution over the mold. The PDMS was made from 1:10 weight ratio of curing agent to PDMS base solution, respectively (Dow Corning Sylgard® 184 #2986922-1104). This step was followed by degassing in a vacuum chamber for 20min. Subsequently, the wafer in the Petri dish was placed on a hot plate at 75°C for 3 h to cure the PDMS. Once the PDMS cured, it was peeled off of the mold. The volume of each PDMS well that formed the array was ~4.24 fL.

Single-molecule experiments

An enzyme concentration of 0.039 nM is equivalent to enclosing 0.1 molecules of enzyme per well (2 μm in diameter and 1.35 μm in height) on average as determined by well size and concentration of enzyme. The volume of each well was ~4.24 fL, and there were a total of over 3,000 wells, excluding wells that had structural artifacts. The EnzChek Protease Assay Kit for Red Fluorescence from Invitrogen (#E-6639) was used. Two microliters of the enzyme at 0.39 nM in 10 nM HEPES buffer was mixed with 17 μL of substrate at 3.06 μM in 1× kit digestion buffer (Tris-HCl). One microliter of 1.0 μm orange polystyrene microspheres (540/560 nm) from Invitrogen (#F-13082) diluted to a final concentration of 2.5×10^4 beads/μL was added to the reaction mixture that had a final volume of 20 μL. The wells were assembled by the following steps. The reaction mixture was placed on a 24 mm × 60 mm glass slide (VWR Micro Cover Glass #48404-454), and we placed the patterned PDMS on top of the glass slide above the solution. The floor of the wells was formed by the glass slide while the PDMS provided the structures for the cylindrical side walls and roof of the wells. To prevent shifting of the PDMS, we taped the PDMS to the glass slide without interfering with the reaction mixture in the wells. We assumed that the wells were filled with the reaction mixture since we had excess fluid surrounding the PDMS-glass slide interface after the initial assembly of the wells. For the prediction of the enclosure of the number of enzymes in each well, we employed the Poisson distribution. With the average number of enzymes enclosed in each well to be 0.1, ~10% of the wells will enclose 1 molecule of enzyme and 90% of them will enclose 0 molecules of enzyme. In a well that contains a single enzyme, the final concentration of the enzyme was 0.39 nM, and that of the substrate was 2.6 μM. The enzyme-to-substrate ratio was 1:6,666 in each well enclosing a single enzyme. CCD images were taken every 3 min for a total duration of 69 min, starting at the time point where the enzyme and the substrate were initially mixed together. The entire experiment was conducted at room temperature. We took 23 CCD images recording at 23 different time points. The exposure time of the CCD images was set to 60 ms. The mercury lamp shutter was closed before and after image exposure.

Image processing

We used MaxIm DL version 2.0× from Diffraction Limited along with the CCD camera to capture the images. To calibrate and analyze the CCD images, we used ImageJ version 1.37 v. From the single-molecule experiments, we obtained images that are processed as follows. First, images were calibrated by correcting bias-, dark-, and flat-field frame noises. Bias frame calibration corrected for variation in camera electronics, dark frame calibration corrected for dark current, and flat-field frame calibration corrected for uneven illumination. We cooled our CCD camera down to −20°C to minimize dark current accumulation in the pixels in the CCD chip. We captured five bias images with the camera shutter closed. Five dark frame images were captured with the same exposure length (60 ms) as the experimental images. We also took five flat-field frame images (600 ms exposure) with 100 nM of BODIPY Texas Red (Invitrogen #D-6116). For the five bias frame images we took, we extracted the median image by using the Z-Projection function for image stacks in ImageJ. We repeated the same median image extraction for each set of the five dark and five flat-field frames. The median flat-field image was normalized to its maximum pixel intensity. The following steps describe our image processing procedure: First, we subtracted the median bias image from an experimental image. Second, we subtracted the resultant bias-frame corrected experimental image with the median dark frame image. Third, we divided the resultant bias frame- and dark frame-corrected image by the normalized median flat-field image. The image processing procedure was performed for both control and experimental groups.

Once the images were calibrated, we further processed them by rotation and cropping in ImageJ. In addition, we subtracted image background in ImageJ by using a rolling ball algorithm with a rolling ball radius of five pixels.[28] Afterward, we adjusted image threshold in ImageJ. The threshold was adjusted by differentiating the wells from the background. The auto threshold runs by taking a test threshold.[29] The average of the pixel values at or below the test threshold is calculated, and the average of the pixel values above the threshold is also computed.[29] Then, a composite average is calculated by averaging two quantities, namely, the average pixel value of the background and the average pixel value of the well.[29] By this method, the threshold is incremented and the process repeats until the threshold is larger than the composite average.[29]

After the threshold was determined, we analyzed the wells (with pixel values above the threshold) by measuring mean pixel intensity of the wells and the corresponding well area. The results were outputted by ImageJ with the number of pixels representing each well and the mean pixel intensity of each well.

Results and Discussion

Ensemble experiments

Results we obtained from the Michaelis-Menten kinetics of α-chymotrypsin using the substrate, casein conjugated to

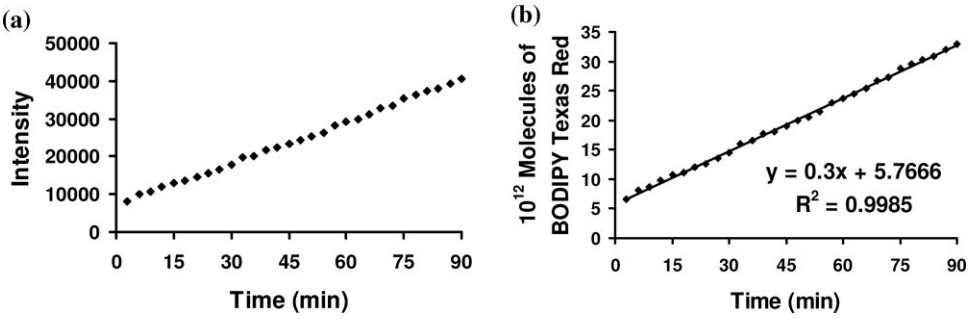

Figure 2. (a) Ensemble Experiment: The intensity of the reaction mixture, containing the enzyme and the substrate, was measured every 3 min for a total of 90 min. [E] = 0.39 nM and [S] = 2.6 μM. (b) Number of BODIPY Texas Red molecules as a function of time. Linear trend line is fitted to display the respective equation and coefficient of determination.

BODIPY Texas Red, allowed us to select for appropriate substrate concentrations for subsequent ensemble and single-molecule experiments.

Ensemble Protease Assays Observing Michaelis-Menten Kinetics. The ensemble kinetics of α-chymotrypsin is described by classical Michaelis-Menten kinetics, which is outlined in the following enzymatic scheme[17,30]:

$$E + S \leftrightarrow ES \leftrightarrow E + P$$

where E represents free enzyme concentration, ES represents the concentration of the bound enzyme to the substrate, and P represents product concentration. Let E_T represent the total concentration of free and bound enzymes. To fulfill the Michaelis-Menten quasi-steady state criteria, E_T is required to be much less than the sum of K_m and S_0.[31] Here, K_m represents the substrate concentration at half the maximum enzymatic reaction velocity, and S_0 refers to the initial substrate concentration.

In our experiment, the initial substrate concentrations were much larger than the initial enzyme concentration (0.39 nM). We used various substrate concentrations on the order of μM as shown in Figure 1 to observe enzyme activity. For each substrate concentration, relative fluorescence intensity was plotted against time (min). By using the dye's linear standard curve [BODIPY Texas Red's standard curve: relative fluorescence units (RFU) vs. [Dye]], we obtained the corresponding concentration of dye with respect to each fluorescence intensity data point measured. By plotting dye concentration in μM against time (min) per enzyme concentration, we obtained the slope (slope = [Dye]/time/[E] in units of μM/min/μM) of each curve for each of the various substrate concentrations we used. The resultant graph of [Dye]/time/[E] as a function of substrate concentration is shown in Figure 1. Equation 1 represents the Lineweaver-Burk equation[32]:

$$\frac{1}{V} = \frac{K_m}{V_{max}}\frac{1}{[S]} + \frac{1}{V_{max}} \quad (1)$$

By rearrangement, enzymatic reaction velocity (V) can be written in the following form:

$$V = \frac{V_{max}[S]}{K_m + [S]} \quad (2)$$

At different substrate concentrations, we obtained different reaction velocities for α-chymotrypsin. We calculated the velocity at each substrate concentration from Eq. 2. Using the Solver function in Microsoft Excel under the tools menu, we set V_{max} and K_m as the variable cells. In addition, we took the difference between the calculated velocities and reaction velocities we obtained from our experiment at various substrate concentrations. Then, we squared the difference in velocity at each substrate concentration and referred to the squared velocity difference as error squared. By minimizing the sum of the error squared (target cell), we determined K_m and V_{max} to be 0.47 μM and 14.75 min^{-1}, respectively. According to previous studies, values of K_m and V_{max} for α-chymotrypsin varied with different substrates and solvents.[33,34] In Figure 1, we presented the mean enzyme reaction velocity from three trials with error bars representing one standard error of mean above and below the mean reaction velocity value.

Ensemble Protease Assays for Comparisons with Single-Molecule Experiments. We analyzed α-chymotrypsin's activity in bulk for direct comparison with the single-molecule experiments. The enzyme, α-chymotrypsin, and the substrate were mixed together at room temperature, having a final concentration of 0.39 nM and 2.6 μM, respectively. As shown in Figure 2a, we recorded the activity of α-chymotrypsin in the form of RFU in the fluorescence microplate reader. In Figure 2a, background-corrected intensity was plotted against time. By using BODIPY Texas Red's standard intensity curve, we constructed Figure 2b, showing the number of dye molecules that contributed to the intensity increase with time. From the slope of Figure 2b, we calculated the rate of product formation, which was 3.0×10^{11} molecules of BODIPY Texas Red per minute. Hence, 12.8 molecules of dye were generated per enzyme molecule per minute. Figure 5 represents the intensity trajectories of 10 individual wells that contained single-enzymes over a total duration of 69 min. By comparing Figures 2 and 5, we observed that ensemble kinetics was not able to detect the intensity distributions of individual molecules. Single-molecule assays not only traced individual enzymes' intensity trajectory, but they also allowed the detection of rare and transient species in a given population of enzymes. It was the distinctive distributions of individual molecules that prompted us to explore the differences between ensemble and single-molecule kinetics.

Single-molecule experiments

The cylindrical wells we used in the single-molecule experiments were fabricated from a silicon mold. The schematic for the fabrication process of the wafer mold is illustrated in Figure 3a. The mold consisted of an array of cylindrical pillars as shown in Figure 3c. The image in Figure 3c shows the resultant structures produced by the

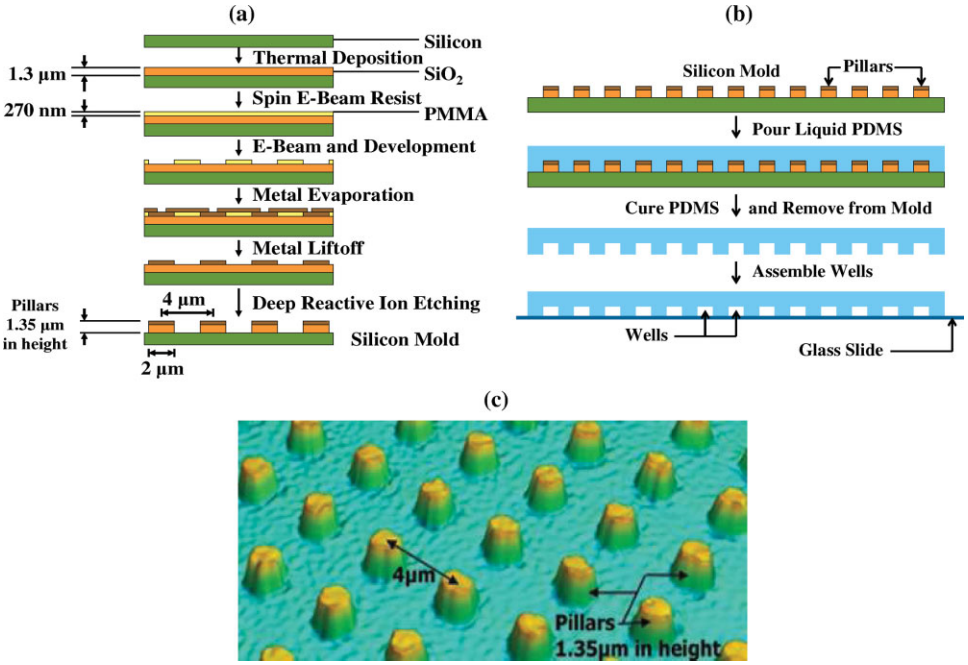

Figure 3. **(a) The side-view of the silicon mold fabrication procedure is shown in this diagram. (b) This image illustrates the assembly of the array of wells. Liquid PDMS is poured over the silicon mold, and the cured PDMS wells that is peeled off of the mold allows for the enclosure of single enzymes. A glass slide is used to form the bottom wall of the wells. (c) This 3-D image generated by the Hyphenated Systems Optical Profiler (HSOP) in the confocal microscope represents a small region of the silicon mold.**

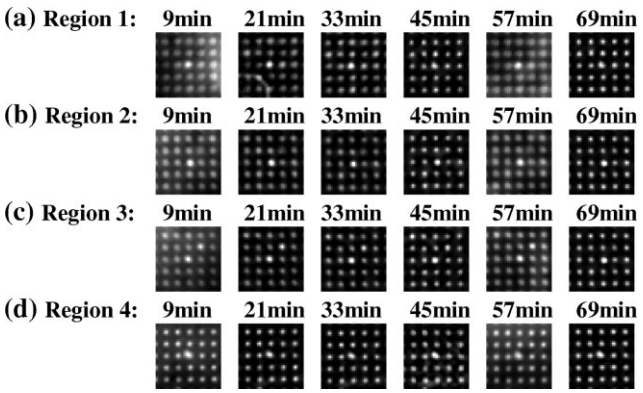

Figure 4. **Single-molecule experiment: CCD images of the array of wells enclosing the reaction mixture.**

Each image consists of a 5 well by 5 well array, which is a small region we selected from the entire array. The intensity of the central well in the 5 × 5 array was observed over time. The array captured in the images are magnified 40× by the objective in our microscope. Each well is 2 μm in diameter, and the distance between the centers of two consecutive wells is 4 μm. In each region, selected, we present the images captured at six points in time: 9, 21, 33, 45, 57, and 69 min. (a) Region 1. (b) Region 2. (c) Region 3. (d) Region 4.

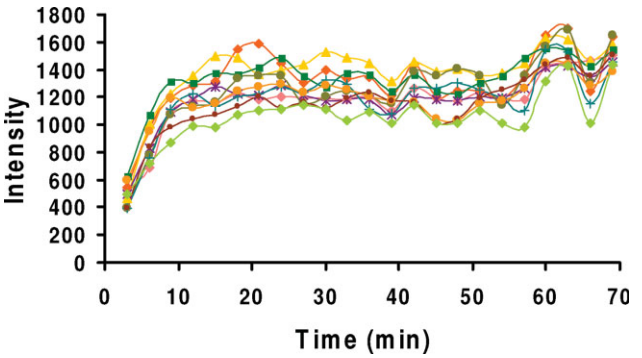

Figure 5. **Single-molecule experiment: Intensity trajectories of 10 individual wells that presumably enclose a single enzyme in each well.**

stepwise fabrication process in Figure 3a. The advantages of using E-beam lithography included the ability to create patterns on the order of submicrons and the elimination of the expense of a photomask.[35,36] After the mold was completed, we used PDMS to create the complementary structures. As shown in Figure 3b, the assembly of the cylindrical wells was achieved by placing PDMS, with patterned structures facing downward, on top of a glass slide. We enclosed our reaction mixture, containing the enzyme and the substrate, between the glass slide and the patterned side of the PDMS. The reaction mixture filled the wells by capillary action in the well-assembly process shown in Figure 3b. We applied light pressure on the PDMS against the glass slide, and the PDMS presses out excess fluid and gases.

After mixing together the enzyme and the substrate and placing them in the wells, a CCD image was taken every 3 min for a total of 69 min. A photo gallery that contains 5 well by 5 well regions of the CCD images captured at six time points (9, 21, 33, 45, 57, and 69 min) is shown in Figure 4. The images shown in Figure 4 were first calibrated to lower background noise. Over time, we traced individual wells, such as the center well in the 5 by 5 well regions of Figure 4, and monitored changes in kinetics. In Figure 5, heterogeneous activity of individual enzymes is reflected by the differences in intensity for 10 individual wells that presumably contain single enzymes in the array. The individual well trajectories in Figure 5 were obtained by taking the mean pixel intensity of each well and recording them at each time point we captured a CCD image. From Figure 5, we observed that the intensity from the product formation of single enzyme activity increased and saturated over time. The

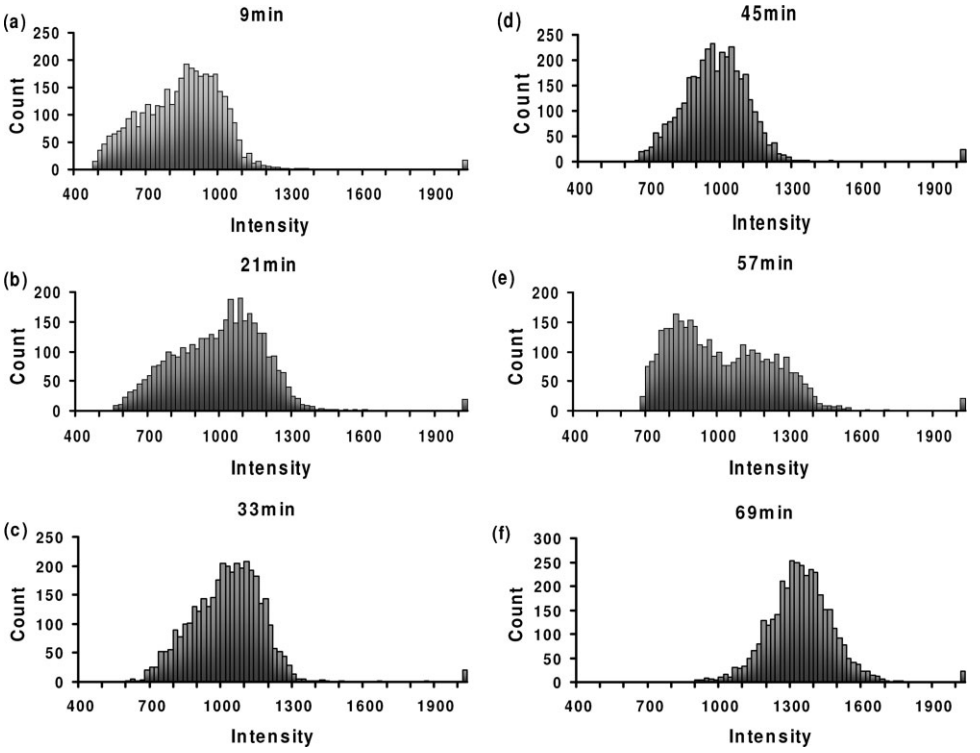

Figure 6. Single-molecule experiment: Well distributions with respect to intensity range.
(a) 9 min, (b) 21 min, (c) 33 min, (d) 45 min, (e) 57 min, and (f) 69 min.

decrease in intensity at 66 min in Figure 5 resulted from focusing challenges in the microscope. Our sample shifted out of focus at 9 and 57 min in Figure 4. Retracting forces of the immersion oil that we used for the oil-immersion objective, temperature changes from heat released from the mercury lamp, and sample vibration were the critical factors that contributed to focus challenges. We improved imperfections of focusing in the microscope by using stage clips to fix our sample to the microscope stage and taping down the PDMS wells to the glass slide.

The advantages of carrying out the protease assay in the array of wells included economical use of chemical reagents, the low cost of the fabrication of the mold, and the reproducibility of PDMS wells once the mold is created. The necessary amount of enzymes and substrates were lower when the assay was miniaturized, and thousands of single-molecule assays were performed in parallel.[35] In addition, we obtained real-time results of the protease assay conducted inside the microwell array. We are confident that at least several hundred wells contained one molecule of enzyme based on the Poisson distribution, which is described in previous literature.[7,37] According to the Poisson distribution in the case where $\mu = 0.1$ molecules of enzyme, ~90% of the total number of wells contained zero molecules of enzyme and 10% of the total number of wells contained 1 molecule of enzyme. We sampled over 3,000 wells. Hence, statistically over 300 wells contained 1 molecule of enzyme.

We further analyzed the images that we had captured for the single-molecule experiments as follows. The mean intensity of each well for the entire single-molecule experiment ranged from 400 to 2,000 relative fluorescence units (RFU). We divided this intensity range into 80 subranges that are 20 RFU apart. At each time point where a CCD image was captured, we counted the number of wells that lay in each subintensity range and constructed a histogram for each time point a CCD image was captured. Six histograms that represent six CCD images captured in six points in time are shown in Figure 6. The shift of well distributions from low to high intensity is evident in Figure 6 from 9 min (Figure 6a) through 69 min (Figure 6f).

Potential complications, such as protein adsorption by PDMS and structural perturbations of proteins in small confined space, may interfere with data interpretation. First, PDMS has been known for its nonspecific protein adsorption. Nevertheless, current literature offers various methods that modify the PDMS surface for the reduction in protein adsorption.[38–40] PDMS has also been known for its hydrophobicity and ability to serve as an impervious boundary to compounds soluble in water.[19] Rondelez et al.[19] have used PDMS as reaction vessels to study horseradish peroxidase and β-galactosidase, and they have shown that β-galactosidase molecules do not bind to the PDMS surface. Furthermore, the hydrogen-bond acceptor groups potentially conducive to protein adsorption in the PDMS structure are likely to be buried by the side chains.[41] Second, the question of whether structural perturbations occur inside confined space is also important. The degree of hydration has been suggested to play a role in an enzyme's activity in aqueous confined space.[42,43] Previous studies have shown that with higher hydration, chymotrypsin's structure in reverse micelles remains unperturbed.[42] When confined in microcapsules, the steric integrity of α-chymotrypsin was not compromised and the thermostability was in fact superior under encapsulation than the free enzyme.[44] It has been shown that only at high temperature ($>>37°C$) and low pH (pH 4.0) does α-chymotrypsin begin to show structural perturbations, lose its active site function, and aggregate to form dimmers.[45,46] We perform our experiments at room

temperature and at pH 7.8, which minimizes the likelihood of structural perturbations due to low pH and high temperatures.

Several other important challenges to our method must be examined. For any method that involves the handling of small working volumes, evaporation is a potential problem. In this project, evaporation of the reaction mixture begins approximately after 2 h. When the reaction mixture evaporates significantly, the sample starts to reveal branch-like streaks of residual fluid. Evaporation is usually not a factor of concern when the experiment is completed within typical time frames of a bioassay, which are a few hours. In addition to evaporation, focus drift is a factor of variation when taking a series of images over time. We carefully focus the image by moving the stage of the microscope, and we look for a consistent plane perpendicular to the *Z*-axis with reference to the bottom and top planes of the wells. Even though the specimen plane that we capture is within the height of the wells, it may well be a different plane from the previous setting. Nevertheless, the plane that we choose will lie within the 1.35 μm height of the wells. A way to overcome this problem is to use a software that is able to automatically correct for focus drift based on reference layers of the specimen.[47] We could increase the precision and consistency of our method by resolving such problems. Another potential problem of a miniaturized assay is the high background. Factors that lower signal-to-background ratio include solvent emission and weak signals from the chromophore of the assay.[48] We work around high background issues by using small working volumes (20 μL) of the reaction mixture, which reduces the volume of solvents compared with bulk assays that use reaction volumes up to 200 μL in 96-well microplate experiments. Because the protease assay that we use also has the ability to quench the fluorescence of the dyes conjugated to the substrate ~98–99% and increase fluorescence signals 50–100 times during enzyme digestion of the substrate, we are confident that our assay has a detectable signal-to-background ratio.[27] In our experiments, we minimize photobleaching by exposing the sample with the mercury lamp only during image capture. Studies have shown that completing the experiment within turnover conditions may also ensure that photobleaching does not affect the accuracy of the experimental findings.[49]

Conclusion

Single-molecule enzymology has the ability to analyze statistical information of single enzyme kinetics that ensemble-averaged kinetics overlooks. The combination of using the array of wells and the protease assay along with the detection technology described in this article presents a potential method for the single-molecule enzymology of α-chymotrypsin. In the future, we might be able to extract more information on α-chymotrypsin by examining how inhibitors influence the single-molecule kinetics of this enzyme.[50]

Acknowledgments

The authors thank Wayne Rasband for his guidance in the use of ImageJ for the applications of this project. This project is supported by the MF3 (Micro/Nano Fluidics Fundamentals Focus) Grant. The authors presented this project as a podium talk at the Annual UC Systemwide Bioengineering Symposium at the University of California, Riverside on June 21, 2008.

Literature Cited

1. Smiley RD, Hammes GG. Single molecule studies of enzyme mechanisms. *Chem Rev*. 2006;106:3080–3094.
2. Min W, English BP, Luo G, Cherayil BJ, Kou SC, Xie XS. Fluctuating enzymes: lessons from single-molecule studies. *Acc Chem Res*. 2005;38:923–931.
3. Walter NG, Huang C-Y, Manzo AJ, Sobhy MA. Do-it-yourself guide: how to use the modern single-molecule toolkit. *Nat Methods*. 2008;5:475–489.
4. Deniz AA, Mukhopadhyay S, Lemke EA. Single-molecule biophysics: at the interface of biology, physics, and chemistry. *J R Soc Interface*. 2008;5:15–45.
5. Xie XS. Optical studies of single molecules at room temperature. *Annu Rev Phys Chem*. 1998;49:441–480.
6. Lu HP. Probing single-molecule protein conformational dynamics. *Acc Chem Res*. 2005;38:557–565.
7. Rissin DM, Gorris HH, Walt DR. Distinct and long-lived activity states of single enzyme molecules. *J Am Chem Soc*. 2008; 130:5349–5353.
8. English BP, Min W, van Oijen AM, Lee KT, Luo G, Sun H, Cherayil BJ, Kou SC, Xie XS. Ever-fluctuating single enzyme molecules: Michaelis-Menten equation revisited. *Nat Chem Biol*. 2006;2:87–94.
9. Qian H, Cooperativity and specificity in enzyme kinetics: a single-molecule time-based perspective. *Biophys J*. 2008;95:10–17.
10. Lee AI, Brody JP, Single-molecule enzymology of chymotrypsin using water-in-oil emulsion. *Biophys J*. 2005;88:4303–4311.
11. Matrai J, Jonckheer A, Joris E, Kruger P, Carpenter E, Tuszynski J, De Maeyer M, Engelborghs Y. Exploration of the activation pathway of deltaalpha-chymotrypsin with molecular dynamics simulations and correlation with kinetic experiments. *Eur Biophys J*. 2008;38:13–23.
12. De Cremer G, Roeffaers MB, Baruah M, Sliwa M, Sels BF, Hofkens J, De Vos DE. Dynamic disorder and stepwise deactivation in a chymotrypsin catalyzed hydrolysis reaction. *J Am Chem Soc*. 2007;129:15458–15459.
13. Bruylants G, Redfield C, Bartik K. Developments in the characterisation of the catalytic triad of alpha-chymotrypsin: effect of the protonation state of Asp102 on the 1H NMR signals of His57. *Chembiochem*. 2007;8:51–54.
14. Champe PC, Harvey RA, Ferrier DR. *Biochemistry*, 3rd ed. Philadelphia: Lippincott Williams & Wilkins; 2005:243–247.
15. Hess GP. Chymotrypsin - chemical properties and catalysis. In: Boyer PD, editor. The Enzymes, 3rd ed. New York, NY: Academic Press; 1971; Chapter 7, Vol. 3, 213–248.
16. Burrell MM, Sweeney PJ, Walker JM. Proteolytic enzymes for peptide production. In: Burrell MM, editor. Enzymes of Molecular Biology. Totowa, NJ; Humana; 1993; Chapter 15, Vol. 16, 277–281.
17. Sola RJ, Griebenow K. Influence of modulated structural dynamics on the kinetics of a-chymotrypsin catalysis. Insights through chemical glycosylation, molecular dynamics, and domain motion analysis. *FEBS J*. 2006;273:5303–5319.
18. Biziulevicius GA, Kislukhina OV, Kazlauskaite J, Zukaite V. Food-protein enzymatic hydrolysates possess both antimicrobial and immunostimulatory activities: a "cause and effect" theory of bifunctionality. *FEMS Immunol Med Microbiol*. 2006;46: 131–138.
19. Rondelez Y, Tresset G, Tabata KV, Arata H, Fujita H, Takeuchi S, Noji H. Microfabricated arrays of femtoliter chambers allow single molecule enzymology. *Nat Biotechnol*. 2005;23:361–365.
20. Jung S-Y, Liu Y, Collier CP. Fast mixing and reaction initiation control of single-enzyme kinetics in confined volumes. *Langmuir*. 2008;24:4439–4442.
21. Shaw AK, Sarkar R, Banerjee D, Hintschich S, Monkman A, Pal SK. Direct observation of protein residue solvation dynamics. *J Photochem. Photobiol A Chem*. 2007;185:76–85.
22. Tan W, Yeung ES. Monitoring the reactions of single enzyme molecules and single metal ions. *Anal Chem*. 1997;69:4242–4248.
23. Yeon WC, Kannan B, Wohland T, Ng V. Colloidal crystals from surface-tension-assisted self-assembly: a novel matrix for single-molecule experiments. *Langmuir*. 2008;24:12142–12149.

24. Comellas-Aragones M, Engelkamp H, Claessen VI, Sommerdijk NA, Rowan AE, Christianen PC, Maan JC, Verduin BJ, Cornelissen JJ, Nolte RJ. A virus-based single-enzyme nanoreactor. *Nat Nanotechnol*. 2007;2:635–639.
25. Yogo T, Urano Y, Ishitsuka Y, Maniwa F, Nagano T. Highly efficient and photostable photosensitizer based on BODIPY chromophore. *J Am Chem Soc*. 2005;127:12162–12163.
26. Gabe Y, Ueno T, Urano Y, Kojima H, Nagano T. Tunable design strategy for fluorescence probes based on 4-substituted BODIPY chromophore: improvement of highly sensitive fluorescence probe for nitric oxide. *Anal Bioanal Chem*. 2006;386:621–626.
27. Jones LJ, Upson RH, Haugland RP, Panchuk-Voloshina N, Zhou M, Haugland RP. Quenched BODIPY dye-labeled casein substrates for the assay of protease activity by direct fluorescence measurement. *Anal Biochem*. 1997;251:144–152.
28. Sternberg SR. Biomedical image processing. *IEEE Comput*. 1983;16:22–34.
29. Rasband WS. ImageJ: image processing and analysis in java. Available at http://rsb.info.nih.gov/ij/.
30. Qian H, Elson EL. Single-molecule enzymology: stochastic Michaelis-Menten kinetics. *Biophys Chem*. 2002;101/102:565–576.
31. Ciliberto A, Capuani F, Tyson JJ. Modeling networks of coupled enzymatic reactions using the total quasi-steady state approximation. *PLoS Comput Biol*. 2007;3:e45.
32. Schnell S, Hanson SM. A test for measuring the effects of enzyme inactivation. *Biophys Chem*. 2007;125:269–274.
33. Clapes P, Adlercreutz P. Substrate specificity of alpha-chymotrypsin-catalyzed esterification in organic media. *Biochim Biophys Acta*. 1991;1118:70–76.
34. Case A, Huskey WP, Stein RL. Enzymatic reaction of silent substrates: kinetic theory and application to the serine protease chymotrypsin. *Biochemistry*. 2003;42:4727–4732.
35. Whitesides GM, Ostuni E, Takayama S, Jiang X, Ingber DE. Soft lithography in biology and biochemistry. *Annu Rev Biomed Eng*. 2001;3:335–373.
36. Gadegaard N, Chen X, Rutten FJM, Alexander MR. High-energy electron beam lithography of octadecylphosphonic acid monolayers on aluminum. *Langmuir*. 2008;24:2057–2063.
37. Lee AI, Brody JP. Diversity in the activity of individual enzymes. *Curr Pharm Biotechnol*. 2005;6:415–425.
38. Makamba H, Hsieh YY, Sung WC, Chen SH. Stable permanently hydrophilic protein-resistant thin-film coatings on poly (dimethylsiloxane) substrates by electrostatic self-assembly and chemical cross-linking. *Anal Chem*. 2005;77:3971–3978.
39. Zheng Z, Jang JW, Zheng G, Mirkin CA. Topographically flat, chemically patterned PDMS stamps made by dip-pen nanolithography. *Angew Chem Int Ed Engl*. 2008;47:9951–9954.
40. Roach LS, Song H, Ismagilov RF. Controlling nonspecific protein adsorption in a plug-based microfluidic system by controlling interfacial chemistry using fluorous-phase surfactants. *Anal Chem*. 2005;77:785–796.
41. Sapsford KE, Ligler FS. Real-time analysis of protein adsorption to a variety of thin films. *Biosens Bioelectron*. 2004;19:1045–1055.
42. Biswas R, Pal SK. Caging enzyme function: alpha-chymotrypsin in reverse micelle. *Chem Phys Lett*. 2004;387:221–226.
43. Priya HM, Shah JK, Asthagiri D, Paulaitis ME. Distinguishing thermodynamic and kinetic views of the preferential hydration of protein surfaces. *Biophys J*. 2008;95:2219–2225.
44. Matsumoto M, Kondo K. Enhanced thermostability of alpha-chymotrypsin enclosed in inorganic microcapsules. *J Biosci Bioeng*. 2001;92:197–199.
45. Banerjee D, Pal SK. Conformational dynamics at the active site of alpha-chymotrypsin and enzymatic acitivity. *Langmuir*. 2008;24:8163–8168.
46. Gilleland MJ, Bender ML. Kinetics of alpha-chymotrypsin dimerization. *J Biol Chem*. 1976;251:498–502.
47. Burglin TR. A two-channel four-dimensional image recording and viewing system with automatic drift correction. *J Microsc*. 2000;200:75–80.
48. Foldes-Papp, Z.; Demel U, Tilz GP. A new concept for ultrasensitive fluorescence measurements of molecules in solution and membrane, Part 1: Theory and a first application. *J Immunol Methods*. 2004;286:1–11.
49. Kuznetsova S, Zauner G, Aartsma TJ, Engelkamp H, Hatzakis N, Rowan AE, Nolte RJM, Christianen PCM, Canters GW. The enzyme mechanism of nitrite reductase studied at single-molecule level. *Proc Natl Acad Sci USA*. 2008;105:3250–3255.
50. Gorris HH, Rissin DM, Walt DR. Stochastic inhibitor release and binding from single-enzyme molecules. *Proc Natl Acad Sci USA*. 2007;104:17680–17685.

Manuscript received Aug. 9, 2008, and revision received Jun. 12, 2009.